

Nonlinear dynamic analysis of dam-foundation interaction under near-fault seismic loading

A. N. Ishmatov¹, M. M. Mirsaidov², A. S. Bykovtsev³, B. Kh Urinov⁴, B. Sh Yuldoshev⁵, I. A. Khazratkulov⁶

^{1, 2, 4, 5, 6}Department of Mechanics and Computer Simulation, National Research University – Tashkent Institute of Irrigation and Agricultural Mechanization Engineers, Tashkent, Uzbekistan

²Institute of Mechanics and Seismic Stability of Structures of the Uzbekistan Academy of Sciences, Tashkent, Uzbekistan

³Regional Academy of Natural Sciences, Port Hueneme, CA, United States

¹Corresponding author

E-mail: ¹alisherishmatov1962@gmail.com, ²mirsaidov1948@mail.ru, ³bykovtsev1@yahoo.com,

⁴bahtierurinov4@gmail.com, ⁵Baxtiyor_yuldashev68@mail.ru, ⁶i.hazratkulov@tiiame.uz

Received 26 February 2026; accepted 30 March 2026; published online 8 June 2026

DOI <https://doi.org/10.21595/vp.2026.26202>



76th International Conference on Vibroengineering in Tashkent, Uzbekistan, April 28-29, 2026

Copyright © 2026 A. N. Ishmatov, et al. This is an open access article distributed under the Creative Commons Attribution License, which permits unrestricted use, distribution, and reproduction in any medium, provided the original work is properly cited.

Abstract. This study presents a methodology for analyzing wave radiation and energy transfer in a dam–foundation–seismic source system. A formulation for heterogeneous viscoelastic media is developed to account for internal damping and energy dissipation in the dynamic response. The method evaluates seismic behavior considering fault-controlled wave propagation and dam-rock interaction. A case study of the Pskem Earth Dam demonstrates the importance of heterogeneity, rheological properties, and fault geometry in seismic safety assessment.

Keywords: dam-foundation interaction, near-fault motion, seismic response, viscoelasticity, wave energy transfer, heterogeneity.

1. Introduction

Seismic simulation of large earth structures requires coupled analysis of the dam-foundation-source system. Material rheology governs wave propagation and energy dissipation. Rock fractures modify seismic motion: dry fractures reduce amplitudes, while fluid-saturated fractures cause frequency-dependent attenuation. Pore-fluid incompressibility also increases effective stiffness and stress concentrations.

Numerous studies have investigated the seismic behavior of hydraulic structures, including the influence of soil conditions [1], advanced numerical schemes for geotechnical earthquake analysis [2], time-domain modeling of dam-reservoir-foundation systems [3], nonlinear dam-reservoir interaction [4], and near-fault pulse-type ground motions [5].

This study considers active faults with dimensions comparable to dominant seismic wavelengths. Unlike simplified elastic models, the proposed approach estimates reductions in elastic moduli and wave velocities under complex radiation. This refinement is critical for high-frequency monitoring and safety assessments of earth dams subjected to near-fault earthquakes.

2. Methods

2.1. Mathematical model

The model includes hydrostatic pressure, free-surface conditions, and foundation constraints. For computational efficiency, the infinite foundation is replaced by a bounded domain preserving wave propagation behavior. Non-reflecting boundary conditions prevent artificial reflections and simulate radiation of wave energy into the far field. The correctness of the formulation is proved

by using the Pskem Earth Dam as a case study. The results indicate that a reliable evaluation of the seismic state necessitates joint consideration of material heterogeneity, dissipative properties, and fault-controlled nonlinear geometric effects.

2.1.1. Mathematical methods for assessing strong ground motion

The adopted approach employs analytical solutions developed by A.S. Bykovtsev [6-11] for complex curvilinear fault systems, including strike-slip and combined slip mechanisms. Synthetic time histories for the Karzhantau fault are shown in Fig. 1. The Pskem Dam in the Tashkent region is used as the case study (computational scheme in Fig. 2). The dam height is 195 m, crest length 1600 m, crest width 12 m, with slope ratios 1:2.4 (upstream) and 1:2 (downstream). The core base width is 130 m, and the reservoir capacity is about 520.000 m³.

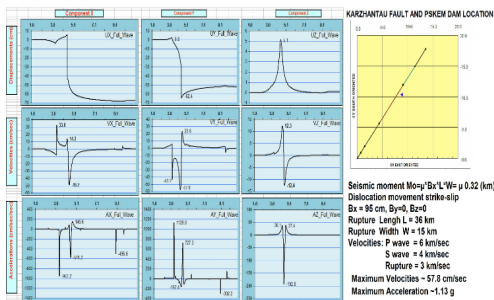


Fig. 1. Synthetic displacement, velocity, and acceleration records for the Pskem Dam section 1 km from the Karzhantau fault ($L = 36$ km, $W = 15$ km, $V = 3$ km/s; $C_p = 6$ km/s, $C_s = 4$ km/s)

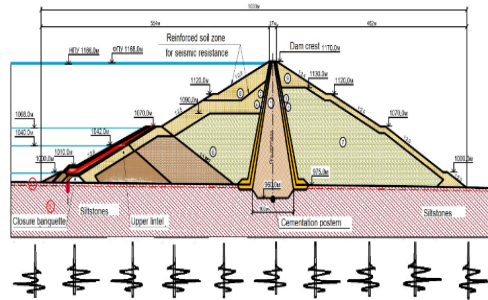


Fig. 2. Finite-element computational scheme used for seismic analysis of the Pskem Dam

2.1.2. Regional tectonics

The seismic hazard of the dam site is controlled by four major fault systems within 20-40 km: Karzhantau, North-Ugam, Ugam-Maydantol, and Pskem. Their geometric and seismogenic characteristics are described in [12].

To evaluate the mechanics of the North-Ugam fault system, analytical solutions based on invariant J-integrals were applied. These invariants allow estimation of driving forces at the fault tip depending on rupture length, fault orientation, external stress state, and mechanical properties of the surrounding medium.

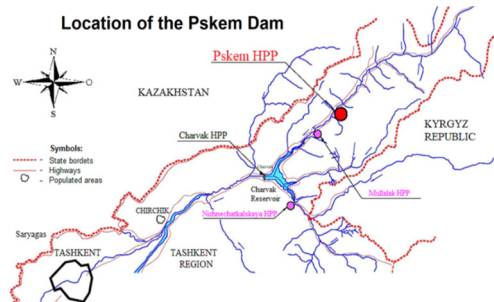


Fig. 3. Geographic location of the Pskem Dam in the Tashkent administrative area

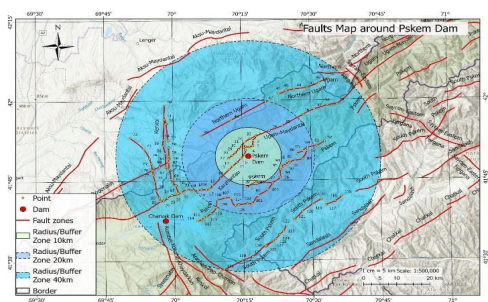


Fig. 4. Regional tectonic framework illustrating major faults in the Pskem Dam region (1:500,000)

2.1.3. Computational model formulation

In this study, a plane heterogeneous model consisting of the dam, foundation, and base is accepted [12], [13]. The computational domain includes a deformable volume $\vec{V} = \vec{V}_1 + \vec{V}_2 + \vec{V}_3 + \vec{V}_4$ and a semi-infinite foundation medium Fig. 5, where all components may exhibit viscoelastic behavior, and the physical properties of their components differ. Body forces and surface loads are included to determine displacements and stresses in the heterogeneous system under dynamic loading. The problems under consideration are posed for a finite domain Fig. 5 of volume $\vec{V} + \vec{V}_5$ (\vec{V}_5 is the volume isolated from a half-space) and bounded by surfaces on which conditions of non-reflective impact are set $\Sigma_1^- + \Sigma_1^+ + \Sigma_2^+$.

The dynamic process is described using the principle of virtual displacements:

$$\delta A = - \int_{V+V_5} \sigma_{ij} \delta \varepsilon_{ij} dV - \int_{V+V_5} \rho_n \ddot{u} \delta \bar{u} dV + \int_{\Sigma_1^- + \Sigma_1^+ + \Sigma_2^+} \sigma_{ij} v_j \delta \bar{u} d\Sigma + \int_V \vec{f} \delta \bar{u} dV + \int_{\Sigma_p} \vec{p} \delta \bar{u} d\Sigma = 0. \quad (1)$$

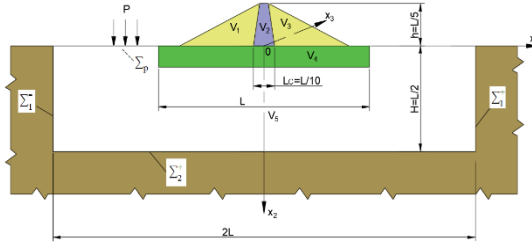


Fig. 5. Computational model of the heterogeneous system

Constitutive relations connect stress tensor σ_{ij} and strain tensor ε_{ij} [13]:

$$\sigma_{ij} = \tilde{\lambda}_n \varepsilon_{kk} \delta_{ij} + 2\tilde{\mu}_n \varepsilon_{ij}. \quad (2)$$

For an elastic material of the n -th element of the system, quantities λ and μ are the Lamé constants; for a viscoelastic material, they are Volterra integral operators [13]:

$$\tilde{\lambda}_n \phi = \lambda_n \left[\phi(t) - \int_0^t \Gamma_{\lambda_n}(t-\tau) \phi(\tau) d\tau \right], \quad \tilde{\mu}_n \phi = \mu_n \left[\phi(t) - \int_0^t \Gamma_{\mu_n}(t-\tau) \phi(\tau) d\tau \right]. \quad (3)$$

For viscoelastic materials, the Lamé constants are replaced by Volterra integral operators \vec{u} :

$$\varepsilon_{ij} = \frac{1}{2} \left(\frac{\partial u_i}{\partial x_j} + \frac{\partial u_j}{\partial x_i} \right). \quad (4)$$

The system also incorporates Cauchy relations Eq. (4) and non-reflecting boundary conditions Eq. (5) to ensure Rayleigh wave propagation across the finite domain boundaries:

$$\vec{x} \in \Sigma_1^\pm: \frac{\partial u_i}{\partial x_1} \pm \frac{1}{c_R} \frac{\partial u_i}{\partial t} = 0, \quad \vec{x} \in \Sigma_2^\pm: u_i = 0. \quad (5)$$

Eq. (5) represents the radiation condition imposed at the artificial boundaries of the truncated computational domain, allowing outgoing waves to propagate without reflection. Displacement components, stress and strain tensors, density parameters, and relaxation operators are defined

according to the viscoelastic formulation described above. The subscripts denote element numbering and spatial coordinates within the heterogeneous domain.

2.2. Computational procedure

2.2.1. Free vibration analysis

The natural dynamic characteristics of the system are obtained by solving the generalized eigenvalue problem:

$$([\bar{K}] - i\omega[\bar{C}] + \omega^2[M])\{\bar{X}\} = 0, \quad (6)$$

where $[M]$ denotes the global mass matrix and $[K]$ represents the effective stiffness matrix incorporating wave energy radiation effects at the artificial boundaries of the truncated computational domain. The frequency-domain representation of Eq. (3) is:

$$\begin{aligned} \tilde{\lambda}_n \phi &\approx \bar{\lambda} \phi = \lambda_n [1 - \Gamma_{\lambda_n}^c(\omega_R) - i\Gamma_{\lambda_n}^s(\omega_R)] \phi, \\ \tilde{\mu}_n \phi &\approx \bar{\mu} \phi = \mu_n [1 - \Gamma_{\mu_n}^c(\omega_R) - i\Gamma_{\mu_n}^s(\omega_R)] \phi, \end{aligned} \quad (7)$$

with corresponding kernel transformations:

$$\Gamma_{\mu_n}^c(\omega_R) = \int_0^\infty \Gamma_{\mu_n}(\tau) \cos \omega_R \tau d\tau, \quad \Gamma_{\mu_n}^s(\omega_R) = \int_0^\infty \Gamma_{\mu_n}(\tau) \sin \omega_R \tau d\tau, \quad (8)$$

$$\Gamma_{\lambda_n}^c(\omega_R) = \int_0^\infty \Gamma_{\lambda_n}(\tau) \cos \omega_R \tau d\tau, \quad \Gamma_{\lambda_n}^s(\omega_R) = \int_0^\infty \Gamma_{\lambda_n}(\tau) \sin \omega_R \tau d\tau. \quad (9)$$

where $\Gamma_{\lambda_n}^s, \Gamma_{\lambda_n}^c, \Gamma_{\mu_n}^s, \Gamma_{\mu_n}^c$ – are the Fourier sine and cosine images of kernels $\Gamma_{\lambda_n}(\tau), \Gamma_{\mu_n}(\tau)$.

Consequently, the eigenvalues in Eq. (6) become complex. The real part defines the oscillation frequency, while the imaginary part represents damping and radiation losses. This approach directly evaluates dissipation within the dam-foundation system. The resulting nonlinear system is solved via iterative root searching and matrix factorization.

2.2.2. Harmonic response analysis

For periodic external excitation, the governing equations are rewritten in the frequency domain, leading to the complex amplitude formulation:

$$([\bar{K}] - i\Omega[\bar{C}] - \Omega^2[M])\{u\} = \{F\} + \{f\}, \quad (10)$$

where Ω is the excitation frequency, $\{X\}$ represents the response amplitudes, $\{f\}$ denotes periodic load components, and $\{F\}$ includes the complete loading vector comprising hydrostatic and body forces. To simulate transient seismic loading typical of near-fault earthquakes, the dynamic equilibrium equations are solved in the time domain:

$$[M]\{\ddot{u}(t)\} + [C]\{\dot{u}(t)\} + [K]\{u(t)\} = \{F\} + \{f(t)\} + \int_0^t \Gamma(t - \tau)[K]\{u(\tau)\}d\tau, \quad (11)$$

with initial conditions:

$$\{u(0)\} = \{u_0\}, \quad \{\dot{u}(0)\} = \{v_0\}. \quad (12)$$

Damping matrix $[C]$ includes both material dissipation effects and boundary energy radiation

contributions. Time integration is performed using the implicit Newmark- β method [13], which provides stable solutions for structural dynamic problems.

3. Results and discussion

Using non-reflecting boundaries Eq. (5), the 2D dynamic response to a transient load (25 m from the base) was analyzed:

$$P(t) = \begin{cases} 100000, & t = 0, \\ -250000t + 100000, & 0 \leq t < 0.4 \text{ sec}, \\ 0, & t \geq 0.4 \text{ sec}. \end{cases} \quad (13)$$

The $P(t)$ load induces non-uniform displacements Eq. (11) synchronized with the wave front. Motion at the crest begins at $t = 0.36$ s, with displacement patterns detailed in Fig. 6.

Fig. 6 shows the horizontal displacement distribution. The wave front propagates from the upstream slope base to the downstream slope, gradually involving the entire structure. Due to diffraction at the contact with the foundation, the zone of isoline "1" (0.0 m) remains immobile. Due to viscoelastic damping, the system stabilizes after the pulse. The isolines are plotted with a step of 0.005 m; the peak displacement reaches 0.042 m.

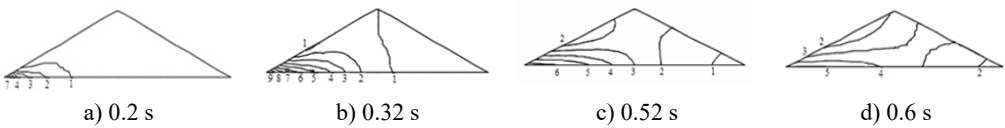


Fig. 6. Horizontal displacement isolines (m) at time steps

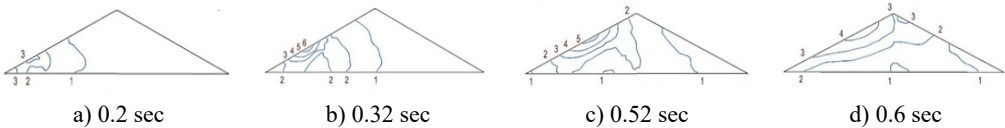


Fig. 7. Isolines of distribution of principal stresses σ_1 in the section of the dam at different time points t

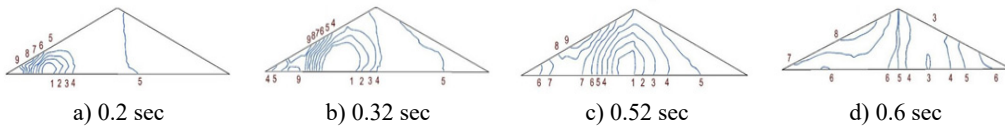


Fig. 8. Isolines of distribution of principal shear stresses σ_{12} in the section of the dam at different time points t

Figs. 7, 8 illustrates the dynamic stress state of the dam. Initially, a tension zone (indicated by isoline 2) forms at the base of the upstream slope and progressively extends deeper into the structure as the wave impacts the dam (see Figs. 7). The principal stresses range from 0.0 MPa (line 1) to 0.3 MPa (line 6), increasing in increments of 0.05 MPa. The maximum shear stresses are concentrated on the surface of the upstream slope, posing a potential landslide hazard. These shear stresses vary from 0.0 MPa (line 5) to ± 0.1 MPa (lines 1 and 9), with increments of 0.025 MPa.

4. Conclusions

This study presents a numerical framework for analyzing the seismic behavior of large earth dams under near-fault ground motion.

The principal contribution of this study can be summarized as follows:

- 1) Seismic source characterization: A database of active faults within 40 km of the Pskem Dam

was compiled to define deterministic earthquake scenarios based on fault segmentation, geometry, and rupture dimensions.

2) Critical near-fault effects: Numerical results indicate that multi-pulse, long-period ground motions significantly drive the nonlinear response of tall earth dams, necessitating the inclusion of pulse-type excitation in seismic hazard assessments.

3) Enhanced energy dissipation modeling: The proposed viscoelastic formulation captures wave energy transfer and internal damping, showing that attenuation depends on the system's dynamic properties and foundation rheology.

Future research should extend this 2D framework to 3D models incorporating complex fault-structure interactions, specifically twisting and mixed-mode ruptures. Further studies on parametric sensitivity, material nonlinearity, and cyclic degradation will refine the reliability of seismic assessments for large hydraulic infrastructure.

Acknowledgements

The authors have not disclosed any funding.

Data availability

The datasets generated during and/or analyzed during the current study are available from the corresponding author on reasonable request.

Conflict of interest

The authors declare that they have no conflict of interest.

References

- [1] M. Zhao, C. Zhang, X. Li, and N. Zhai, "Dynamic responses of concrete-face rockfill dam to different site conditions under near-fault earthquake excitation," *Buildings*, Vol. 13, No. 10, p. 2410, Sep. 2023, <https://doi.org/10.3390/buildings13102410>
- [2] G. Elia and M. Rouainia, "Advanced dynamic nonlinear schemes for geotechnical earthquake engineering applications: a review of critical aspects," *Geotechnical and Geological Engineering*, Vol. 40, No. 7, pp. 3379–3392, Apr. 2022, <https://doi.org/10.1007/s10706-022-02109-6>
- [3] Y. Qu, D. Chen, L. Liu, E. T. Ooi, S. Eisenträger, and C. Song, "A direct time-domain procedure for the seismic analysis of dam-foundation-reservoir systems using the scaled boundary finite element method," *Computers and Geotechnics*, Vol. 138, p. 104364, Oct. 2021, <https://doi.org/10.1016/j.compgeo.2021.104364>
- [4] L. Pelecanos, S. Kontoe, and L. Zdravković, "The effects of dam-reservoir interaction on the nonlinear seismic response of earth dams," *Journal of Earthquake Engineering*, Vol. 24, No. 6, pp. 1034–1056, Jun. 2020, <https://doi.org/10.1080/13632469.2018.1453409>
- [5] A. C. Altunisik and H. Sesli, "Effect of near-fault ground motion with pulse signal on dynamic response of dam-reservoir-foundation systems," *Journal of the Croatian Association of Civil Engineers*, Vol. 74, No. 12, pp. 1059–1083, Jan. 2023, <https://doi.org/10.14256/jce.1573.2016>
- [6] A. S. Bykovtsev, "Propagation of complex discontinuities with piecewise constant and variable velocities along curvilinear and branching trajectories," *Journal of Applied Mathematics and Mechanics*, Vol. 50, No. 5, pp. 620–628, Jan. 1986, [https://doi.org/10.1016/0021-8928\(86\)90037-7](https://doi.org/10.1016/0021-8928(86)90037-7)
- [7] A. S. Bykovtsev and D. B. Kramarovskii, "The propagation of a complex fracture area, the exact three-dimensional solution," *Journal of Applied Mathematics and Mechanics*, Vol. 51, No. 1, pp. 89–98, Jan. 1987, [https://doi.org/10.1016/0021-8928\(87\)90043-8](https://doi.org/10.1016/0021-8928(87)90043-8)
- [8] A. S. Bykovtsev, "Numerical modeling of the wave field in the coastal zone of a step-propagating curved fault and analysis of high-temperature processes," (in Russian), *News of the USSR Academy of Sciences, Earth Physics*, Vol. 3, pp. 3–16, 1989.
- [9] A. S. Bykovtsev and J. S. Semenova, "On fault system interaction," in *Computational Mechanics '95*, pp. 2129–2134, Jan. 1995, https://doi.org/10.1007/978-3-642-79654-8_354

- [10] A. S. Bykovtsev and D. B. Kramarovsky, "The influence of faults. On the stability of the slopes of the Muruntau quarry," (in Russian), *Mining Bulletin of Uzbekistan*, Vol. 2, pp. 64–68, 1998.
- [11] A. S. Bykovtsev, "Calculation of synthesized seismic impacts from earthquakes of various types and faults with different directions of motion along faults within 10 km from the fault zone (BAS-KDB-1)," (in Russian), Republic of Uzbekistan, 2024.
- [12] B. K. U. M. M. Mirsaidov, A. S. Bykovtsev, S. Shukurova, A. N. Ishmatov, and I. O. Khazratkulov, "Strength of the system 'structure-foundation-earthquake source' under seismic impacts generated by active faults around the Pskem earth dam taking into account wave energy carryover," in *The World Congress on Advances in Structural Engineering and Mechanics (ASEM25)BEXCO, Busan, Korea, August 11-14, 2025*, Aug. 2025.
- [13] M. M. Mirsaidov, T. Z. Sultanov, and D. F. Rumi, "An assessment of dynamic behavior of the system "structure – foundation" with account of wave removal of energy," (in Russian), *Magazine of Civil Engineering*, Vol. 39, No. 4, pp. 94–105, Jun. 2013, <https://doi.org/10.5862/mce.39.10>